Journal of Fluorine Chemistry 130 (2009) 38–44

Contents lists available at ScienceDirect

Journal of Fluorine Chemistry

journal homepage: www.elsevier.com/locate/fluor

Heat-transport properties of molten fluorides: Determination from first-principles

Mathieu Salanne [a,b,*], Christian Simon [a,b], Pierre Turq [a,b], Paul A. Madden [c]

[a] UPMC Univ Paris 06, UMR 7612, LI2C, 4 Place Jussieu, Paris F-75005, France
[b] CNRS, UMR 7612, LI2C, Paris F-75005, France
[c] School of Chemistry, University of Edinburgh, Edinburgh EH9 3JJ, UK

ARTICLE INFO

Article history:
Received 29 February 2008
Received in revised form 21 May 2008
Accepted 3 July 2008
Available online 23 July 2008

Keywords:
Molten salt
FLINAK
Fluorozirconate
Molecular dynamics
Heat-transfer properties
Force-fitting

ABSTRACT

The construction of an interaction potential for mixtures of LiF, NaF, KF and ZrF_4 on a purely first-principles basis is described. Many-body interactions are included *via* a polarization term. The predictions of the heat-transfer properties of two mixtures, LiF–NaF–KF (FLiNaK) and NaF–ZrF_4, are then compared with experimental values. Values for the densities, thermal expansions, heat capacities and viscosities are compiled into figures of merits in order to compare the suitability of those molten salts to serve as primary or secondary coolants in a nuclear reactor.

1. Introduction

The Generation IV International Forum consists of a consortium of 10 nations which is planning the nuclear reactors of tomorrow. Six reactors concepts have been chosen and research and development programmes have been initiated. One of them, the molten salt reactor (MSR), is investigated for use as either waste incinerator or thorium cycle system [1–3]. In this concept, molten fluorides are used as both the fuel and coolant (and also as a solvant in the integrated waste reprocessing unit). Molten salts could also be used as primary coolant in another concept, the advanced high-temperature reactor (AHTR) [4]. This reactor design utilizes the same graphite-matrix fuel of helium-cooled reactors, but provides cooling with a high-temperature molten fluoride. To evaluate the suitability of several molten salts to serve as primary or secondary coolants, a screening logic was established by Grimes [5]. First, elements that could possibly compose the molten salt must have a small cross-section (values < 1 barn) at the wanted neutron temperature (for example, thermal neutrons in the AHTR). Then molten salt candidates must exhibit chemical stability at $T > 800\,^{\circ}C$, be stable under intense radiation, melt at useful temperatures ($< 525\,^{\circ}C$) without being volatile and be compatible with high-temperature alloys and graphite. In the MSR, the molten salt must also dissolve useful quantities of fertile and fissile material.

Based on those considerations, three "families" of molten fluorides were selected as possible coolants in the AHTR [6]. The first of them contains mixtures of alkali fluoride salts, while the second and third, respectively, are ZrF_4 and BeF_2 containing salts. Even for these systems, important gaps appear in the databases of heat-transfer properties. Two approaches have been used to obtain those quantities: experimental measurement and prediction through extrapolation. Accurate measurements can be made for the density, the melting point, the vapor pressure and the viscosity, but among those properties, only the density can successfully be predicted by extrapolation. Few measurements of the heat capacity have been made and the predictive capability for this quantity is very limited, so that the uncertainty in that quantity remains important. Finally, the thermal conductivity data is very poor because of the difficulties encountered in determining it by either approach.

In this article we show how simulations could help completing the existing databases for heat-transfer properties. Our

* Corresponding author at: UPMC Univ Paris 06, UMR 7612, LI2C, 4 Place Jussieu, Paris F-75005, France. Tel.: +33 144273265.
E-mail address: mathieu.salanne@upmc.fr (M. Salanne).

0022-1139/$ – see front matter © 2008 Elsevier B.V. All rights reserved.
doi:10.1016/j.jfluchem.2008.07.013

approach consists in performing molecular dynamics (MD) simulations of ionic materials. The interaction potentials necessary to carry on the calculations are determined from a fully first-principles procedure, so that no other property but the density of pure compounds are needed. The procedure was already tested and validated on the experimentally well-characterized molten fluoride mixture of LiF with BeF_2, whose properties were successfully described by our simulations [7–9]. Here we show how accurate estimations of the mixture densities, viscosities and heat capacities can be determined, making our approach a powerful predictive tool.

We begin by detailing the different terms in the interaction potentials involved in the MD calculations and describing the determination of the corresponding parameters for melts containing F^-anions and Li^+, Na^+, K^+ and Zr^{4+} cations. The second part of the paper accounts for the determination of the above-mentioned heat-transfer properties for two molten salt mixtures, LiF–NaF–KF and NaF–ZrF_4, and comparison with their experimental values. In the final section, we discuss the prospects for rendering such calculations on other materials and extending its scope to the computation of thermal conductivity.

2. Results and discussion

2.1. Interaction potentials

The potential is best described as the sum of four different components: charge–charge, dispersion, overlap repulsion and polarization [10]. The first three components are purely pairwise additive; first the charge–charge term is:

$$\upsilon^{q-q} = \sum_{i<j} \frac{q^i q^j}{r^{ij}} \tag{1}$$

where q^i is the charge on ion i, and formal charges are used throughout. The dispersion component includes dipole–dipole and dipole–quadrupole terms

$$\upsilon^{\text{disp}} = \sum_{i<j} \left((1 - f_6(b^{ij} r^{ij})) \frac{C_6^{ij}}{(r^{ij})^6} + (1 - f_8(b^{ij} r^{ij})) \frac{C_8^{ij}}{(r^{ij})^8} \right) \tag{2}$$

where C_6^{ij} (C_8^{ij}) is the dipole–dipole (dipole–quadrupole) dispersion coefficient, and $(1 - f_n)$ are Tang–Toennies dispersion damping functions [11], describing the short-range penetration correction to the asymptotic multipole expansion of dispersion [12]($f_n(0) = 1$ and $f_n(\infty) = 0$). These functions take the form

$$f_n(x) = \mathrm{e}^{-x} \sum_{k=0}^{n} \frac{x^k}{k!} \tag{3}$$

and the parameter, b^{ij}, represent the distance at which the correction begins to be taken into account. The third term of the interaction potential, the repulsion overlap component, is given by

$$\upsilon^{\text{rep}} = \sum_{i<j} B^{ij} \mathrm{e}^{-a^{ij} r^{ij}}. \tag{4}$$

The polarization part of the potential includes charge–dipole and dipole–dipole terms:

$$\upsilon^{\text{pol}} = \sum_{i,j} q^i \mu_\alpha^j (1 - c^{ji} f_4(b_D^{ij} r^{ij})) \mathbb{T}_\alpha^{(1)} - q^j \mu_\alpha^i (1 - c^{ij} f_4(b_D^{ij} r^{ij})) \mathbb{T}_\alpha^{(1)} - \sum_{i,j} \mu_\alpha^i \mu_\beta^j \mathbb{T}_{\alpha\beta}^{(2)} + \sum_i \frac{1}{2\alpha^i} |\vec{\mu}^i|^2 \tag{5}$$

Here $\mathbb{T}_\alpha^{(1)}$ and $\mathbb{T}_{\alpha\beta}^{(2)}$ are the charge–dipole and dipole–dipole interaction tensors and α^i is the polarizability of ion i. Again, we have to include some short-range effects, which are due to the high compression of the ions in condensed ionic materials. In fact, any fluctuation in the shape of the local coordination shell of an ion lowers its symmetry, allowing the electron density to relax into the space created [13], therefore inducing an additional dipole moment. These short-range induction effects can be examined in electronic structure calculations in which the total moment in a locally distorted coordination geometry of a high symmetry crystal is calculated and the part attributable to induction by the interionic coulomb potential removed. The effects are very large and for anions, the short-range multipoles for a given distortion oppose the coulombic ones [14,15]. These short-range induction effects are straightforwardly included through the use of damping functions similar to the ones used in the dispersion term. Here c^{ij} is a parameter that reflects the amplitude of this damping at ion j due to the presence of i and b_D^{ij} again is a range parameter.

The instantaneous values of the dipole moments ($\{\vec{\mu}^i\}_N$) are obtained by minimization of υ^{pol} with respect to these variables: they will therefore depend on the instantaneous positions of neighboring ions and consequently change at each timestep in an MD run. The interaction potential can therefore be seen to contain three additional degrees of freedom (induced dipoles), which describe the state of the electron charge density of the ions. When calculating the forces on the ions in an MD simulation, these electronic degrees of freedom should have their "Born–Oppenheimer" values, which minimize the total potential energy, for every atomic configuration. We search for the ground state configurations of these degrees of freedom at each time step, using a conjugate gradient routine [16], after an initial prediction from their values at the preceding timestep, with Car–Parrinello dynamics [17,18]. The dynamics is thus similar to the so-called Born–Oppenheimer first-principles molecular dynamics, as implemented, for example, in the CPMD code [19].

We perform an Ewald summation of all electrostatic interactions and also of dispersion [20]. Thus, all those interactions are free from truncation errors. The short-range repulsion, which is an exponentially decaying function of distance, is however truncated beyond a distance equal to half the simulation cell length.

2.2. First-principles parametrization

The various parameters involved in the interaction potential described above were determined through a "force-fitting" procedure. It had already been successfully applied in the case of oxides, although with a more complicated interaction potential form and a detailed description has been given recently [21,22]. Here we will focus on features specific to the fluoride systems of interest.

In the force-fitting process, we first generated several representative condensed-phase configurations for LiF, NaF, KF, ZrF_4, LiF–ZrF_4 and NaF–ZrF_4, each containing roughly 60–130 ions in periodic boundary conditions by using an approximate interaction potential (the number of ions in each configuration is given in Table 3 of Section 4). We performed first-principles electronic structure calculations on those configurations within the planewave DFT formalism. These are analyzed to give the components of the force and the dipole on each ion in each configuration. The details of those calculations are given in Section 4 of this article. We then fit the potential by varying the parameters in the potential to minimize the difference between the first-principle forces and dipoles and those predicted by the potential model for the given atomic arrangement.

First, we determine the polarization set of parameters $\{\chi_P\} = \{\{\alpha^i\}_{N_{\text{spec}}}, \{b_D^{ij}\}_{N_{\text{spec}}^2}, \{c^{ij}\}_{N_{\text{spec}}^2}\}$ by fitting the dipoles predicted by the model to the first-principles calculated ones ($\{\vec{\mu}^i_{fp}\}_N$). This was

done by minimizing the objective function

$$A_P(\{\chi_P\}) = \sum_{i,A} \frac{|\vec{\mu}^i(\chi_P) - \vec{\mu}^i_{fp}|^2}{|\vec{\mu}^i_{fp}|^2} \quad (6)$$

and allowing the set of parameters $\{\chi_P\}$ to vary. The sum over A represents the sum over all atomic configurations included in the fit. To optimize the objective function, a nongradient simplex method was used [23].

The set of forces obtained directly from CPMD were then used to minimize the objective function

$$A_F(\{\chi_{SR}\}) = \sum_{i,A} \frac{|\vec{F}^i(\chi_{SR}) - \vec{F}^i_{fp}|^2}{|\vec{F}^i_{fp}|^2} \quad (7)$$

as a function of the set $\{\chi_{SR}\} = \{\{B^{ij}\}_{N^2_{spec}}, \{a^{ij}\}_{N^2_{spec}}\}$ of short-range potential parameters while holding the polarization parameters fixed. The quality of these fits is illustrated on Fig. 1. The abcissa in these plots represent the index of an ion in a given configuration and the ordinate gives values for the x-component of either the dipole moment (top) or the force (bottom) on that ion. The circles give the first-principles values and the line the values predicted by the fitted potential. The data on Fig. 1 is given for all the configurations in a row so it corresponds to alterance of anions and more or less polarizable cations; this is why important differences appear between successive blocks of values. Uniformly good fits across the range of configurations appear for the forces while the dipole moment seems to be underestimated for several ions (those with high dipole moment values). Still, the values of the objective functions were $A_P = 0.0696$ and $A_F = 0.0879$, which we regard as indicating good fits and shows that the dipoles are overall well-represented (the Li^+ ions, which had null dipole moments, were not included in the calculation of A_P).

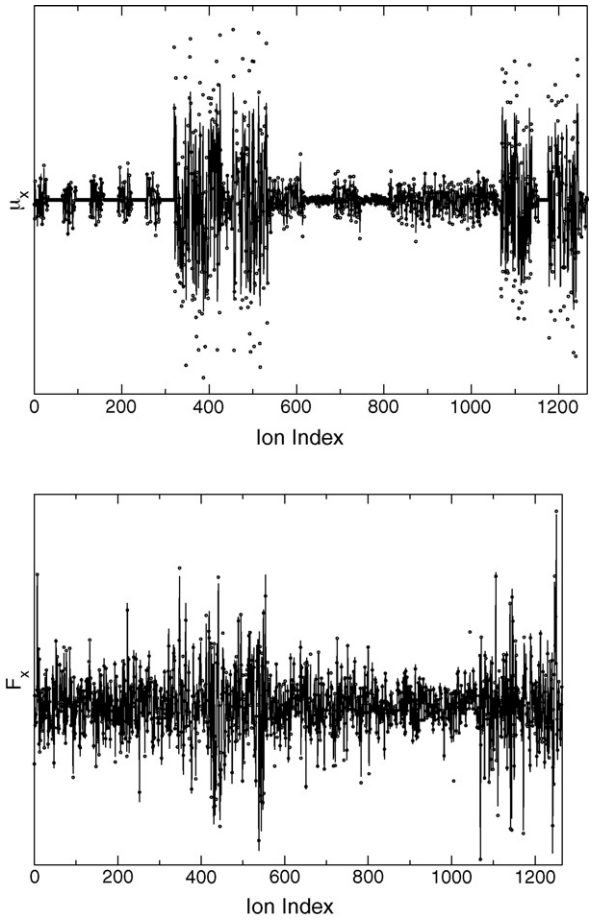

Fig. 1. Quality of the fits of the x-components of the forces and dipole moments on the ions to those obtained from the first-principles calculations. The solid lines show the prediction of our polarizable ion model potential, and the circles the results from the first-principles calculations. Data is given for all the configurations listed in Table 3 in a row.

As presented so far, the procedure for constructing the potential has a refreshingly hands-off aspect—the decisions about parameters and the sophistication of the potential are indicated by the force-fitting on a very large body of data. Unfortunately, there is one aspect of the potential development which has been skated over so far to which this does not apply. This concerns the representation of the dispersion interactions between the ions. The basic problem is that the representation of the dispersion interactions in the DFT calculations we are using to parameterize the potential is essentially uncontrolled. This problem has been noted in studies of atomic and molecular systems [24]. It is frustrating that it should be an important issue in ionic materials because the dispersion energies are a *tiny* fraction of the interaction energies of pairs of ions; nevertheless, the *relative* energies of two phases are often sufficiently sensitive to the dispersion interactions to have a substantial effect on transition pressures, etc. Thus we have determined the dispersion parameter (b^{ij}, C^{ij}_6 and C^{ij}_8) in order to reproduce the experimental density of the pure compounds. We chose the density because this quantity is sensitive and because it is already well-known for numerous systems, either liquids or solids. Although the dispersion parameters are therefore determined empirically, the values obtained are similar to those which have been obtained from high-quality (coupled cluster) quantum chemical calculations on these ions [25].

Values for the different parameters are given in Table 1. One should note that the cation–cation short-range parameters were not fitted because these species mainly interact through their formal charges. The fitted values for the polarizabilities were of 1.17 $Å^3$ for F^-, 0.15 $Å^3$ for Na^+, 0.74 $Å^3$ for K^+ and 0.42 $Å^3$ for Zr^{4+}. The Li^+ ions are considered to be not polarizable.

2.3. Heat-transfer properties

As it was built, the interaction potential allows us to simulate any mixture involving F^- anions and Li^+, Na^+, K^+ and Zr^{4+} cations. In this section we focus on two systems, LiF–NaF–KF and NaF–ZrF_4, at the respective compositions of 46.5–11.5–42 and 57–43 mole percents. They belong to the families of molten fluorides to be investigated as primary coolants of the AHTR (mixtures of alkali

Table 1
Parameters of the interaction potential (atomic units)

Ion pair ij	B^{ij}	a^{ij}	C^{ij}_6	C^{ij}_6	b^{ij}	b^{ij}_D	c^{ij}	c^{ji}
F^-–F^-	282.3	2.444	15.0	150.0	1.9	1.0	0.0	0.0
F^-–Li^+	18.8	1.974	1.2	12.2	1.9	1.83	1.34	0.0
F^-–Na^+	52.8	1.974	13.3	88.2	1.9	1.84	2.54	−0.19
F^-–K^+	138.8	2.043	3.9	38.7	1.9	1.75	2.50	−0.31
F^-–Zr^{4+}	72.2	1.791	33.5	335.0	1.9	1.84	1.72	−0.94
Li^+–Li^+	5.0	1.0	0.1	1.0	1.9	1.0	0.0	0.0
Li^+–Na^+	5.0	1.0	1.1	7.0	1.9	1.0	0.0	0.0
Li^+–K^+	5.0	1.0	0.3	3.2	1.9	1.0	0.0	0.0
Li^+–Zr^{4+}	5.0	1.0	2.7	27.4	1.9	1.0	0.0	0.0
Na^+–Na^+	5.0	1.0	11.7	51.8	1.9	1.0	0.0	0.0
Na^+–K^+	5.0	1.0	3.4	22.8	1.9	1.0	0.0	0.0
Na^+–Zr^{4+}	5.0	1.0	29.6	197.1	1.9	1.0	0.0	0.0
K^+–K^+	5.0	1.0	1.0	10.0	1.9	1.0	0.0	0.0
K^+–Zr^{4+}	5.0	1.0	8.7	86.6	1.9	1.0	0.0	0.0
Zr^{4+}–Zr^{4+}	5.0	1.0	75.0	750.0	1.9	1.0	0.0	0.0

fluorides and ZrF_4 containing salts) and they are particularly interesting because of their low melting points: the LiF–NaF–KF mixture melts at 454 °C while the NaF–ZrF_4 one melts at 530 °C. We will successively present the simulation results for the densities, thermal expansions, heat capacities and viscosities of these molten fluorides, and provide a comparison with experimental results when they are available. Finally, we will discuss the suitability of the salts through the use of figures of merit, which provide an easy way to compare the heat-transfer properties of several candidate coolants.

2.3.1. Density

Fluid density is one of the most straightforwardly obtained properties. Firstly, a lot of experimental work has been performed, and secondly a simple method based on additive molar volumes has proven to be efficient for the prediction of the salt densities at new compositions [26].

We can determine the liquid densities from the mean value of the volume of the simulation cell at a given temperature in the *NPT* ensemble simulations. Our results are given in Fig. 2 where they are compared to the experimental values.

Two different sets of experimental values are available for the LiF–NaF–KF density. One can see that our values are equal to Mellors and Senderoff ones [28], while Grimes et al. values are a bit higher [27]. In the case of NaF–ZrF_4, our data are consistent with the experimental values reported in reference [6]. This shows that the density of the mixtures can be reproduced with a good accuracy by our model. As the dispersion term parameters were chosen to reproduce the density of the pure systems, such an agreement can be expected from the empirical finding of additive molar volumes.

The variation of density with temperature is linear. From the data of Fig. 2, we determined the following equations:

- LiF–NaF–KF: $\rho = 2.603 - 6.69 \times 10^{-4} T$
- NaF–ZrF_4: $\rho = 3.935 - 9.18 \times 10^{-4} T$

where T is expressed in K and ρ in g cm^{-3}.

2.3.2. Thermal expansion

The thermal expansion of a material corresponds to the volume change in response to a change in temperature. It is given by

$$\beta = \frac{1}{\upsilon}\left(\frac{\partial V}{\partial T}\right)_P \quad (8)$$

$$\beta = -\frac{1}{\rho}\left(\frac{\partial \rho}{\partial T}\right)_P \quad (9)$$

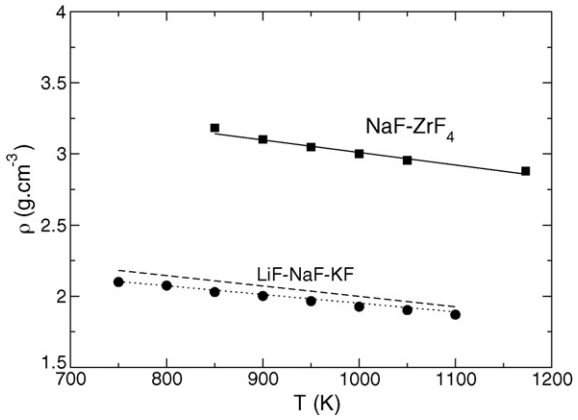

Fig. 2. Experimental (lines) and simulated (symbols) densities of LiF–NaF–KF and NaF–ZrF_4 melts. For LiF–NaF–KF, two experimental results are shown: dashed line values are from Ref. [27] and dotted line values from Ref. [28].

It was computed from the temperature variation of density in LiF–NaF–KF and NaF–ZrF_4 mixtures; the result is shown on Fig. 3. The good agreement between the computed densities and the experimental ones ensures us that those thermal expansions are accurate. In the studied range of temperature, the variations with temperature again are roughly linear, and the following expressions could be determined:

- LiF–NaF–KF: $\beta = 2.32 \times 10^{-4} + 1.136 \times 10^{-7} T$
- NaF–ZrF_4: $\beta = 2.12 \times 10^{-4} + 0.925 \times 10^{-7} T$

where β is given in K^{-1}.

2.3.3. Heat capacity

The massic enthalpies H^m of the melts have also been obtained from the *NPT* runs. These quantities are plotted versus temperature on Fig. 4. The massic heat capacities C_p^m can be determined from:

$$C_p^m = \left(\frac{\partial H^m}{\partial T}\right)_P, \quad (10)$$

The variation of H^m is very small for both mixtures and linear; thus on the range of temperatures used in this study we can consider C_p^m to be constant. We obtained values of 1.769 J g^{-1} K^{-1} for the LiF–NaF–KF mixture and 1.066 J g^{-1} K^{-1}, in good agreement with the experimental values [29] of, respectively, 1.883 J g^{-1} K^{-1} and 1.172 J g^{-1} K^{-1}. This good agreement is remarkable, as no thermodynamic data was at any point included to the force-fitting procedure. Most of the available experimental values for molten salts heat capacities were determined with very crude calorimeters compared to today's available material. Our MD simulations provide an alternative way to predict efficiently and at low cost the heat capacities for any other molten salt compositions.

2.3.4. Viscosity

The shear viscosity is a measure of the resistance of a fluid to being deformed by shear stress. In MD simulations, it can be calculated as the time integral of the shear stress autocorrelation function:

$$\eta = \frac{\beta}{\upsilon}\int_0^\infty \langle \sigma_{\alpha\beta}(t)\sigma_{\alpha\beta}(0)\rangle \, dt \quad (11)$$

It is important to run the simulations for a long time to get sufficiently good statistics. Moreover, the stress autocorrelation function is averaged over its five independent components (σ_{xy}, σ_{xz}, σ_{yz}, σ_{xx-yy}, $\sigma_{2zz-xx-yy}$), as shown for the LiF–NaF–KF mixture at

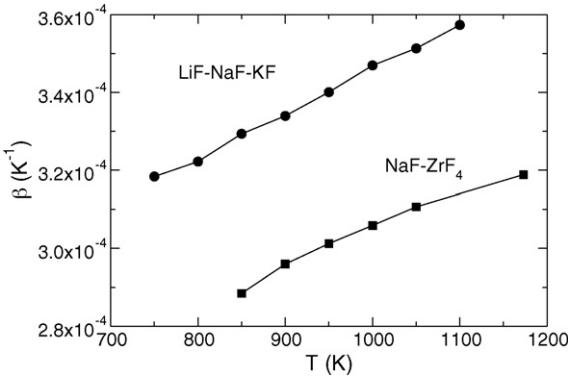

Fig. 3. Thermal expansions of LiF–NaF–KF and NaF–ZrF_4 melts.

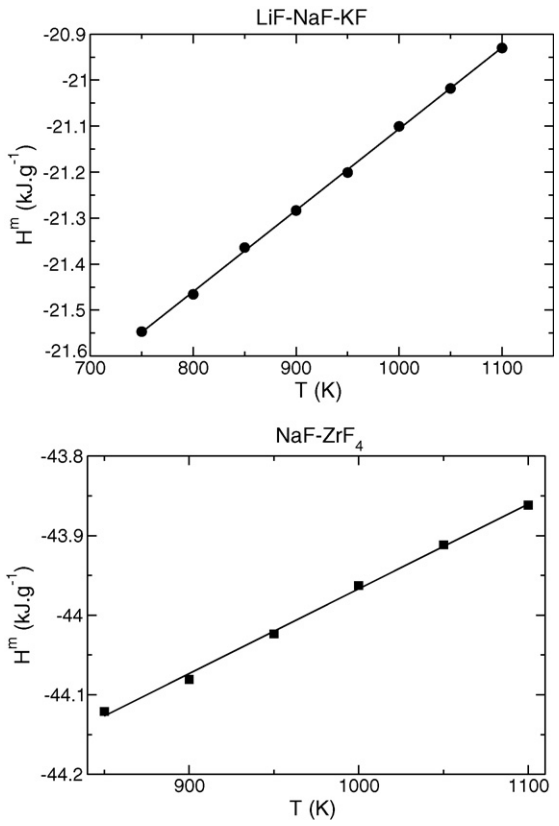

Fig. 4. Massic enthalpy of LiF–NaF–KF and NaF–ZrF_4 melts.

a temperature of 800 K on Fig. 5. The viscosity is then given by the plateau value of the running integral.

Good agreement is again observed between experiments and simulation. One should note that, except for data from reference [30], the experimental lines plotted on Fig. 6 correspond to correlation equations (with an exponential decrease with temperature), and thus they do not reflect the important error bars resulting from the measurements. For example, at 973 K, Williams et al. report a viscosity of 5.1 cP for the NaF–ZrF_4 at the same composition as in our study, which compares very well with our value of 5.2 cP. The higher viscosity of NaF–ZrF_4 reflects the formation of complex fluorozirconate species in that melt; a

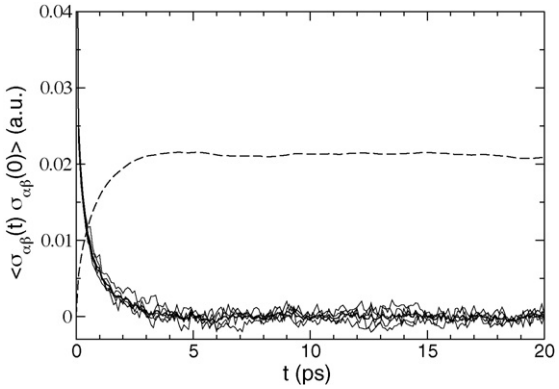

Fig. 5. Stress tensor autocorrelation functions for the LiF–NaF–KF melt at 800 K. The various components (*xy*, *xz*, *yz*, *xx–yy* and *2zz–xx–yy*) are showed as thin lines, while the average over all components corresponds to the thick line. The integral, from which is determined the viscosity through Eq. (11), is represented with a dashed line.

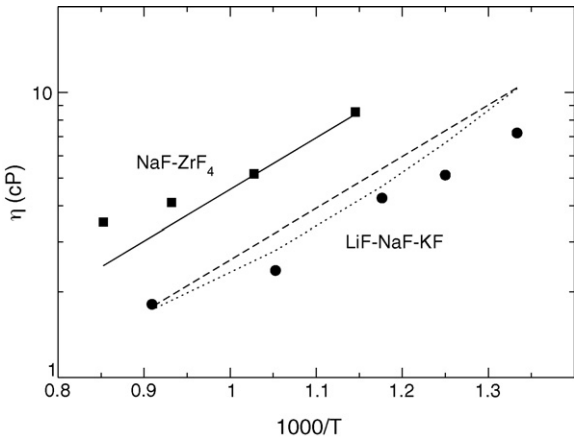

Fig. 6. Comparison of the computed and experimental viscosities. Simulation results are given by the squares (NaF–ZrF_4) and circles (LiF–NaF–KF), while the lines correspond to the experimental values. The straight line corresponds to a 50–50 mol percent NaF–ZrF_4mixture [6], while the dashed and dotted line are two different measures for the LiF–NaF–KF mixture, respectively given in references [27] and [30].

discussion on the relationship between the structure of another molten fluoride, LiF–BeF_2, and its viscosity can be found in reference [31]. There are a number of mixtures for which no viscosity data exists; the ability of our model to determine this quantity for two very different mixtures like LiF–NaF–KF and NaF–ZrF_4 strongly suggests that MD with appropriate interaction potentials is a viable way to complete the existing databases.

2.3.5. Figures of merit

All the quantities we have computed so far cannot be taken individually to determine the ability of a molten salt to transfer heat; depending on the nature of the flow, they will be of more or less importance. To determine the performance of a given coolant, it is useful to use generalized heat-transfer metrics. Several figure of merits (FOM) have been proposed by Bonilla to evaluate the properties of molten fluorides as coolants [32]:

- Forced convection, turbulent regime:

$$\mathrm{FOM1} = \frac{\eta^{0.2}}{\rho^2 (C_p^{\mathrm{m}})^{2.8}} \tag{12}$$

- Natural convection, turbulent regime:

$$\mathrm{FOM2} = \left(\frac{\eta^{0.2}}{\beta \rho^2 (C_p^{\mathrm{m}})^{1.8}} \right)^{0.36} \tag{13}$$

- Natural convection, laminar regime:

$$\mathrm{FOM3} = \left(\frac{\eta}{\beta \rho^2 C_p^{\mathrm{m}}} \right)^{0.5} \tag{14}$$

The smaller the values of these FOMs, the better they perform as coolants. Their form clearly shows that the viscosity has to be minimized while the other quantities have to be maximized. This demonstrates that important cancellation effects will occur in our mixtures: for example, adding $ZrF_4$to a salt will enhance its density but also its viscosity. The values we obtained for the three FOMs at a temperature of 973 K for LiF–NaF–KF and NaF–ZrF_4 mixtures are displayed in Table 2.

For all the flow régimes, smaller FOM values are obtained for LiF–NaF–KF. The difference is more important in forced convection

Table 2
Figures of merits of the two melts at 973 K

Mixture	FOM1	FOM2	FOM3
LiF–NaF–KF	0.063	8.01	31.45
NaF–ZrF_4	0.126	8.98	41.74

(FOM1) than in natural convection. This shows that this melt has better heat-transfer properties; this does not mean that it should automatically be preferred as a coolant since other parameters also are of great importance.

3. Conclusions

We have shown how an interaction potential for mixtures of LiF, NaF, KF and ZrF_4 mixtures may be parameterized from first-principles. This polarizable ion model potential could reproduce the first-principles calculated forces and dipoles for a set of configurations that spanned different first-solvation shell structure of the ions.

We then demonstrated the ability of the resulting simulations to determine various terms involved in the coolants' classification through the use of figure of merits. As a first example, we chose the LiF–NaF–KF and NaF–ZrF_4 mixtures, for which we could obtain densities, thermal expansions, heat capacities and viscosities in good agreement with former experimental results. This set of properties involve different chemical and thermodynamic mechanisms. Future work should focus on the prediction of these quantities for other salts like LiF–ThF_4, for which very few experimental data is available. It is important to note that nowadays an important experimental work is aimed at the determination of structural [33–39] and electrochemical [40–43] properties of the molten fluorides, but only one group is involved in studies concerning their thermal properties [44–46](some work has also been done on the system LiF–NaF–BeF_2 in the framework of the fusion energy reactors [47]). In the future simulations will be of particular importance to complete the gaps in the necessary databases.

Among the thermal properties of interest, the thermal conductivity is the most bad known. Experiments are difficult to carry on and no empirical estimation technique has proven to be useful. For the moment, our simulations could not provide this quantity: because of the inclusion of the many-body polarization effects, no good expression for the heat flux has yet been written. When those effects are not taken into account, i.e. when the pair potential only consists in pairwise additive terms, such a calculation is possible and this work has already been successfully performed in molten NaCl [48,49]. Future work should focus on finding an appropriate way to compute thermal conductivities in molten fluorides.

4. Experiments

4.1. Planewave DFT calculations

Several configurations of LiF, NaF, KF, ZrF_4, LiF–ZrF_4 and NaF–ZrF_4 were obtained in the liquid phase. The corresponding number of atoms are given in Table 3. The atoms in these configurations sampled a wide range of thermally distorted environments and solvation shells, and the aim was that, by using a sufficiently large and varied set of such configurations, a transferable potential would be obtained. First-principles DFT calculations were performed using the CPMD code [19]. We used Goedecker pseudopotentials [50] for all ions together with the PBE [51] exchange-correlation functional, and a kinetic energy cutoff of 100 Ry to ensure a high degree of convergence of the forces.

Table 3
Number of ions in the configurations used for the force-fitting procedure

Configuration	N_{F^-}	N_{Li^+}	N_{Na^+}	N_{K^+}	$N_{Zr^{4+}}$
1	32	32	0	0	0
2	32	32	0	0	0
3	32	32	0	0	0
4	32	32	0	0	0
5	32	32	0	0	0
6	108	0	0	0	27
7	108	0	0	0	27
8	64	0	64	0	0
9	64	0	64	0	0
10	64	0	0	64	0
11	64	0	0	64	0
12	72	15	0	0	12
13	72	0	15	0	12

The electronic wavefunction derived from these calculations are the Kohn–Sham orbitals, which are delocalized throughout the simulation cell, and periodic. In order to associate orbitals with each ion, from which we may calculate dipole moments, we switched to a localized representation of the wavefunction, *via* a Wannier transformation [52] of the Kohn–Sham eigenvectors. If the condition of maximal localization [53] is enforced, a set of Wannier orbitals is obtained which provides a picture of the electron distribution around ions polarized by the electrostatic field of the surrounding environment and is easily interpretable from a chemical point of view. The dipole moment of an individual ion is calculated from the center of the charge of the subset of maximally localized Wannier functions which localize in the vicinity of it [54,55].

4.2. Molecular dynamics simulations

Molecular dynamics simulations were performed on two molten salt mixtures, LiF–NaF–KF and NaF–ZrF_4. The interaction potential parameters we used were the ones obtained from the force-fitting procedure; they are listed in Table 1. The simulation cells contained the following number of ions:

(1) LiF–NaF–KF mixture: 216 F^-, 100 Li^+, 25 $Na^+$and 91 K^+
(2) NaF–ZrF_4 mixture: 229 F^-, 57 Na^+ and 43 Zr^{4+}

Both systems were first simulated in the *NPT* ensemble following the method described by Martyna et al. [56], with a pressure fixed at 0 GPa. Temperatures varied from 750 K to 1100 K for LiF–NaF–KF and from 850 K to 1100 K (with a temperature step of 50 K between each simulation). We chose a time step of 0.5 fs and the total simulation time was of 100 ps at each temperature.

Then we performed simulations in the *NVT* ensemble, enforcing the canonical ensemble sampling through the use of the Nosé–Hoover chain thermostat method [57,58]. The simulations temperatures were 750 K, 800 K, 850 K, 950 K and 1100 K for LiF–NaF–KF; 873 K, 973 K, 1073 K and 1173 K for NaF–ZrF_4. The cell volumes were chosen to match the 0 GPa pressure density curves obtained from the *NPT* simulations. The time step was the same as before but the simulation time was much longer, 2 ns, to ensure good statistics for the computation of the viscosities.

Acknowledgements

The authors would like to acknowledge the financial support of PACEN (Programme sur l'Aval du Cycle et l'Energie Nucléaire) through PCR-RSF and GDR PARIS programmes.

References

[1] C.L. Brun, J. Nucl. Mater. 360 (2007) 1–5.
[2] L. Mathieu, D. Heuer, R. Brissot, C. Garzenne, C.L. Brun, D. Lecarpentier, E. Liatard, J. Loiseaux, O. Meplan, E. Merle-Lucotte, A. Nuttin, E. Walle, J. Wilson, Prog. Nucl. Energy 48 (7) (2006) 664–679.
[3] J. Vergnes, D. Lecarpentier, Nucl. Eng. Des. 216 (1–3) (2002) 43–67.
[4] C. Forsberg, Prog. Nucl. Energy 47 (1–4) (2005) 32–43.
[5] W. Grimes, Nucl. Appl. Technol. 8 (2) (1970) 137–155.
[6] D. Williams, L. Toth, K. Clarno, Tech. Rep. ORNL/TM-2006/12, Oak Ridge National Laboratory, Oak Ridge, TN (2006).
[7] R. Heaton, R. Brookes, P. Madden, M. Salanne, C. Simon, P. Turq, J. Phys. Chem. B 110 (23) (2006) 11454–11460.
[8] M. Salanne, C. Simon, P. Turq, R. Heaton, P. Madden, J. Phys. Chem. B 110 (23) (2006) 11461–11467.
[9] M. Salanne, C. Simon, P. Turq, P. Madden, C. R. Chim. 10 (2007) 1131–1136.
[10] P. Madden, M. Wilson, Chem. Soc. Rev. 25 (5) (1996) 339–350.
[11] K. Tang, J. Toennies, J. Chem. Phys. 80 (8) (1984) 3726–3741.
[12] A. Stone, The theory of intermolecular forces, Oxford University Press, Oxford, 1996.
[13] P. Fowler, P. Madden, Phys. Rev. B 31 (8) (1985) 5443–5455.
[14] C. Domene, P. Fowler, M. Wilson, P. Madden, Mol. Phys. 100 (24) (2002) 3847–3865.
[15] P. Jemmer, M. Wilson, P. Madden, P. Fowler, J. Chem. Phys. 111 (5) (1999) 2038–2049.
[16] W. Press, B. Flannery, S. Teukolski, W. Vetterling, Numerical Recipes, 2nd edition, Cambridge University Press, 1992.
[17] R. Car, M. Parrinello, Phys. Rev. Lett. 55 (22) (1985) 2471–2474.
[18] R. Vuilleumier, Lect. Notes Phys. 703 (1) (2006) 223–285.
[19] The CPMD consortium, CPMD Version 3.10, http://www.cpmd.org., MPI Für Festkörperforschung and the IBM Zurich Research Laboratory.
[20] Z. Chen, T. Cagin, W. Goddard III, J. Comput. Chem. 18 (11) (1997) 1365–1370.
[21] A. Aguado, L. Bernasconi, S. Jahn, P. Madden, J. Chem. Soc., Faraday Discuss. 124 (2003) 171–184.
[22] P. Madden, R. Heaton, A. Aguado, S. Jahn, J. Mol. Struct.: THEOCHEM 771 (2006) 9–18.
[23] F. James, M. Roos, Comp. Phys. Commun. 10 (6) (1975) 343–367.
[24] X. Wu, M. Vargas, S. Nayak, V. Lotrich, G. Scoles, J. Chem. Phys. 115 (19) (2001) 8748–8757.
[25] P. Fowler, P. Knowles, N. Pyper, Mol. Phys. 56 (1) (1985) 83–95.
[26] W. Grimes, Tech. Re ORNL-3913, Oak Ridge National Laboratory, Oak Ridge, TN (1966).
[27] W. Grimes, D. Cuneo, F. Blankenship, G. Keilholtz, H. Poppendiek, M. Robinson, Fluid Fuel Reactors, Addison-Weslay, Reading, MA, 1958, chapter 12.
[28] G. Mellors, S. Senderoff, in: Proceedings of the Australian Conference on Electrochemistry, vol. 1, 1963, pp. 578–598.
[29] G. Janz, Molten Salts Handbook, Academic Press, NY, 1967.
[30] K. Torklep, H. Oye, J. Chem. Eng. Data 25 (1980) 16–17.
[31] M. Salanne, C. Simon, P. Turq, P. Madden, J. Phys. Chem. B 111 (18) (2007) 4678–4684.
[32] C. Bonilla, Nuclear Engineering Handbook, 1958, pp. 9–90, chapter 6.5.
[33] A. Rollet, C. Bessada, Y. Auger, P. Melin, M. Gailhanou, D. Thaudière, Nucl. Instrum. Methods Phys. Res., Sect. B 226 (2004) 447–452.
[34] A. Rollet, C. Bessada, A. Rakhmatullin, Y. Auger, P. Melin, M. Gailhanou, D. Thiaudière, C. R. Chim. 7 (2004) 1135–1140.
[35] A. Rollet, A. Rakhmatullin, C. Bessada, Int. J. Thermophys. 26 (2005) 1115–1126.
[36] C. Bessada, A. Rollet, A. Rakhmatullin, I. Nuta, P. Florian, D. Massiot, C. R. Chim. 9 (2006) 374–380.
[37] C. Bessada, A. Rakhmatullin, A. Rollet, D. Zanghi, J. Nucl. Mater. 360 (1) (2007) 43–48.
[38] S. Watanabe, H. Matsuura, H. Akatsuka, Y. Okamoto, P. Madden, J. Nucl. Mater. 344 (1–3) (2005) 104–108.
[39] S. Watanabe, A. Adya, Y. Okamoto, N. Umesaki, T. Honma, H. Deguchi, M. Horiuchi, T. Yamamoto, S. Nogushi, K. Takase, A. Kajinami, T. Sakamoto, M. Hatcho, N. Kitamura, H. Akatsuka, H. Matsuura, J. Alloys Compd. 408–412 (2006) 71–75.
[40] P. Chamelot, L. Massot, C. Hamel, C. Nourry, P. Taxil, Proceedings of the 7th International Symposium on Molten Salts Chemistry & Technology 2 (2005) 615–618.
[41] C. Hamel, P. Chamelot, A. Laplace, E. Walle, O. Dugne, P. Taxil, Electrochem. Acta 52 (12) (2007) 3995–4003.
[42] J. Finne, G. Picard, S. Sanchez, E. Walle, O. Conocar, J. Lacquement, J.-M. Boursier, D. Noel, J. Nucl. Mater. 344 (2005) 165–168.
[43] H. Groult, A. Barhoun, H.E. Ghallali, S. Borensztjan, F. Lantelme, J. Electrochem. Soc. 155 (2) (2008) E19–E25.
[44] J. van der Meer, R. Konings, H. Oonk, J. Nucl. Mater. 357 (1–3) (2006) 48–57.
[45] J. van der Meer, R. Konings, D. Sedmidubsky, A. van Genderen, H. Oonk, J. Chem. Thermodyn. 38 (11) (2006) 1260–1268.
[46] J. van der Meer, R. Konings, J. Nucl. Mater. 360 (1) (2007) 16–24.
[47] G. Fukuda, P. Peterson, D. Olander, J. Prausnitz, Fluid Phase Equilib. 255 (1) (2007) 1–10.
[48] N. Galamba, C. de Castro, J. Ely, J. Chem. Phys. 120 (18) (2004) 8676–8682.
[49] N. Galamba, C. de Castro, J. Ely, J. Chem. Phys. 126 (20) (2007) 204511.
[50] S. Goedecker, M. Teter, J. Hutter, Phys. Rev. B 54 (3) (1996) 1703–1710.
[51] J. Perdew, K. Burke, M. Ernzerhof, Phys. Rev. Lett. 77 (1996) 3865–3868.
[52] E. Blount, Solid State Phys. 13 (1962) 305–373.
[53] N. Marzari, D. Vanderbilt, Phys. Rev. B 56 (20) (1997) 12847–12865.
[54] L. Bernasconi, M. Wilson, P. Madden, Comp. Mater. Sci. 22 (1–2) (2001) 94–98.
[55] L. Bernasconi, P. Madden, M. Wilson, Phys. Chem. Commun. 5 (1) (2002) 1–11.
[56] G. Martyna, D. Tobias, M. Klein, J. Chem. Phys. 101 (5) (1994) 4177–4189.
[57] S. Nosé, Mol. Phys. 52 (1984) 255–268.
[58] G. Martyna, M. Klein, M. Tuckerman, J. Chem. Phys. 97 (4) (1992) 2635–2643.